Supplementary information:

Lieb lattices formed by real atoms on Ag(111) and their lattice constant dependent electronic properties

Xiaoxia Li†, Qili Li†, Tongzhou Ji, Ruige Yan, Wenlin Fan, Bingfeng Miao, Liang Sun, Gong Chen, Weiyi Zhang, Haifeng Ding*

†These authors contribute equally to this work

*Corresponding author: hfding@nju.edu.cn

S-1. TIGHT-BINDING METHOD

The band structure of the Lieb lattice can be derived from a tight-binding model. In it, we consider the overlap among *s*-states electrons. The Hamiltonian of the system is $H = \sum_i \varepsilon_i a_i^+ a_i - t\sum_{\langle i,j\rangle}(a_i^+ a_j + H.C.) - t'\sum_{\langle\langle i,j\rangle\rangle}(a_i^+ a_j + H.C.)$ with t and t' as the nearest-neighboring (NN) and the next-nearest-neighboring (NNN) overlap energy, respectively.

We set the onsite energy to be ε_0 for both corner- and edge-sites, and the lattice constant to be *2r*. Then the matrix form of the Hamiltonian of the system is:

$$\mathbf{H} = \begin{pmatrix} \varepsilon_0 & -2t\cos(k_x r) & -2t\cos(k_y r) \\ -2t\cos(k_x r) & \varepsilon_0 & -4t'\cos(k_x r)\cos(k_y r) \\ -2t\cos(k_y r) & -4t'\cos(k_x r)\cos(k_y r) & \varepsilon_0 \end{pmatrix}. \quad (1)$$

The energy eigenvalues are obtained by solving the secular equation:

$$\det\left|\mathbf{H} - \varepsilon \mathbf{I}_{3\times 3}\right| = \begin{vmatrix} \varepsilon_0 - \varepsilon & -2t\cos(k_x r) & -2t\cos(k_y r) \\ -2t\cos(k_x r) & \varepsilon_0 - \varepsilon & -4t'\cos(k_x r)\cos(k_y r) \\ -2t\cos(k_y r) & -4t'\cos(k_x r)\cos(k_y r) & \varepsilon_0 - \varepsilon \end{vmatrix} = 0. \quad (2)$$

For the case of $t' = 0$, the Hamiltonian can be simplified as:

$$\mathbf{H} = \begin{pmatrix} \varepsilon_0 & -2t\cos(k_x r) & -2t\cos(k_y r) \\ -2t\cos(k_x r) & \varepsilon_0 & 0 \\ -2t\cos(k_y r) & 0 & \varepsilon_0 \end{pmatrix}. \quad (3)$$

The eigenvalues can be obtained as:

$$\begin{cases} \varepsilon_1 = \varepsilon_0 \\ \varepsilon_2 = \varepsilon_0 - 2t\sqrt{(\cos^2(k_x r) + \cos^2(k_y r))}. \\ \varepsilon_3 = \varepsilon_0 + 2t\sqrt{(\cos^2(k_x r) + \cos^2(k_y r))} \end{cases} \quad (4)$$

ε_1 is a flat band. ε_2 and ε_3 are two dispersive bands. Then we employ the numerical integral method to obtain local density of states (LDOS) spectra. The corresponding LDOS spectra at the edge- and corner-sites demonstrate that there are two peaks at $E_l = \varepsilon_0 - 2t$ and $E_h = \varepsilon_0 + 2t$ at corner site, and one additional peak appears at $E_m = \varepsilon_0$ due to the flat band. Therefore, the NN overlap energy can be obtained as:

$$t = \frac{E_h - E_m}{2} \text{ or } \frac{E_m - E_l}{2}. \quad (5)$$

When $t' \neq 0$, the flat band bends near the Brillouin zone center, while it remains flat from M to Γ. Thus, it can still result a peak in the LDOS of edge-site with a small shift from ε_0 (Fig. S1(a)). The corresponding LDOS maps are shown in Fig. S1(b). Note that considering the lifetime effect of surface state electrons, we added a broadening of $0.2t$ in the LDOS calculation.

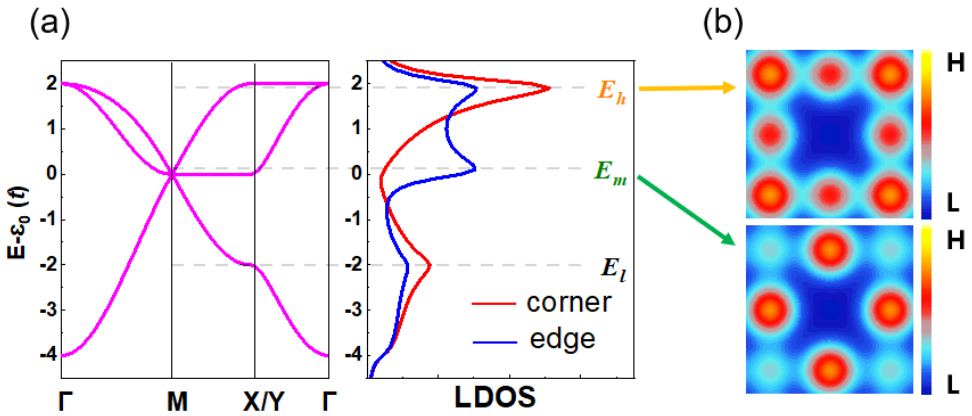

Fig. S1: (a) Calculated electronic band structure and LDOS of a Lieb lattice with t = 100 meV and $t' = 0.5t$ via tight-binding method. (b) Corresponding LDOS maps at E_h (upper) and E_m (lower).

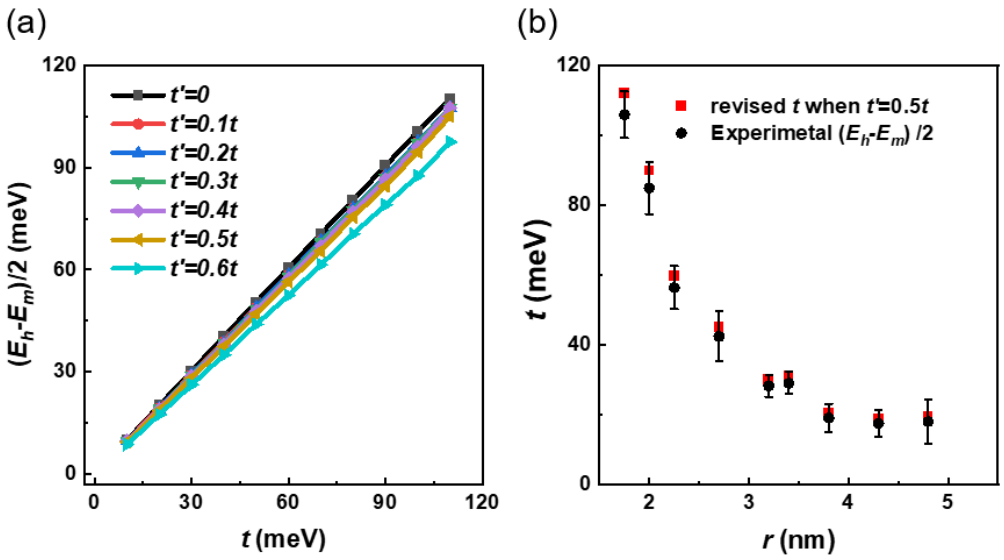

Fig. S2: (a) The calculated influence of t' on the estimation of t with the proposed method. (b) Comparison of the revised t and the experimentally obtained ones.

To evaluate the influence of t', we calculate $\frac{E_h - E_m}{2}$ as a function of t for different t' from 0 to 0.6t. As shown in Fig. S2(a), the overlap energy is exactly $\frac{E_h - E_m}{2}$ for $t' = 0$. As for $t' \neq 0$, the value of $\frac{E_h - E_m}{2}$ has a small deviation from t. It is, however, still within the experimental error bar, as shown in Fig. S2(b). Thus, we can approximately obtain:

$$t \approx \frac{E_h - E_m}{2}. \tag{6}$$

In addition, the tight-binding calculation is based on the assumption that the wavefunction of the neighboring atoms, φ_i and φ_j are orthogonal. Namely, $s_{ij} = \langle \varphi_i | \varphi_j \rangle = 0$. In ref. [18], the authors, however, obtained s = 0.15 for artificially atoms built by quantum well states with a separation of ~1.28 nm. In our experiment, the minimum separation is about 1.75 nm. It can be anticipated that s should be smaller than 0.15 in our case due to its decay property with increasing

separation. Thus, we performed the calculations for *s* from 0 to 0.15. As shown in the figure below, it has little influence on the positions of the peaks. Therefore, it has no influence on our main conclusion.

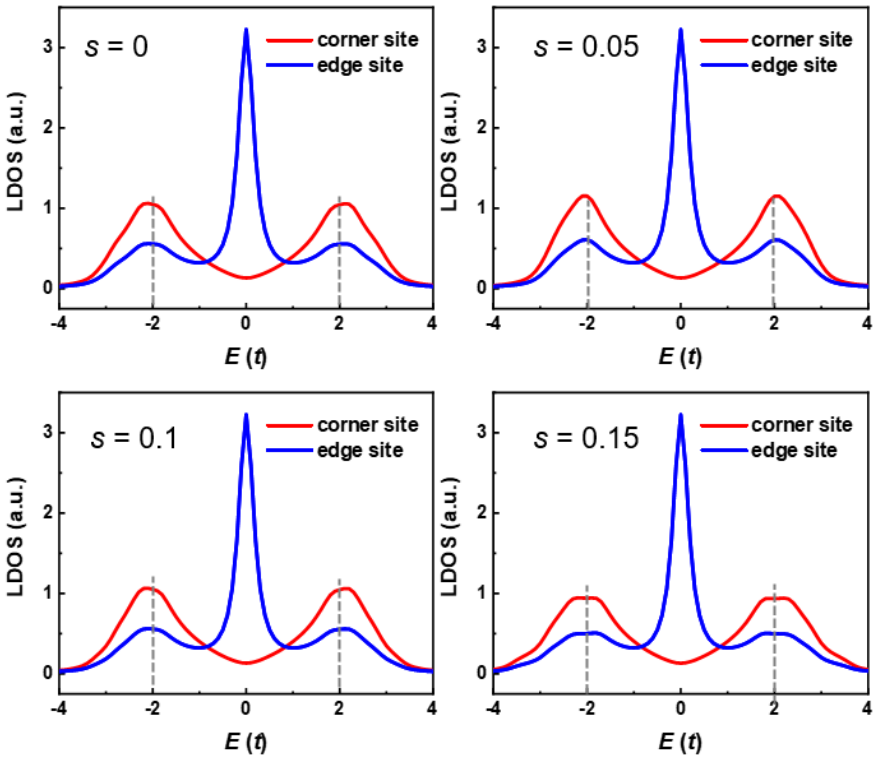

Fig. S3: The influence of *s* on the positions of characteristic LDOS peaks of a Lieb lattice.

S-2. GREEN'S FUNCTION METHOD

We consider a 4×4 Lieb lattice on the Ag(111) surface. According to the T-matrix method [1-4], the Green's function is

$$G(r,r';E)=G_0(r,r';E)+\sum_{i,j=1}^{N}G_0(r,r_i;E)T(r_i,r_j;E)G_0(r_j,r';E), \quad (7)$$

where $G_0(r,r';E) = -i\pi\rho_s H_0^{(1)}(k|r-r'|)$ is the free two-dimensional Green's function. $H_0^{(1)}(x)$ gives the zeroth-order Hankel function of the first kind and ρ_s is the density of state of the surface state. $T(r_i,r_j;E)$ is the T-matrix determined by Dyson's equation, which contains the information about the propagation between the impurities *i* and *j*:

$$T(r_i,r_j;E) = V_i\delta_{i,j} + V_i\sum_{l=1}^{N} G_0(r_i,r_l;E)T(r_l,r_j;E). \tag{8}$$

V is the scattering potential of the adatom to the surface state.

In matrix form, $\mathbf{T} = \mathbf{V} + \mathbf{V}\mathbf{G_0}\mathbf{T}$, thus we obtain $\mathbf{T} = \mathbf{V}(\mathbf{I} - \mathbf{V}\mathbf{G_0})^{-1}$ [5], where

$$\mathbf{V} = \begin{pmatrix} \mathbf{V_1} & 0 & \cdots & 0 \\ 0 & \mathbf{V_2} & \cdots & 0 \\ \vdots & \vdots & \ddots & \vdots \\ 0 & 0 & \cdots & \mathbf{V_N} \end{pmatrix}, \tag{9}$$

and

$$\mathbf{G}_0 = \begin{pmatrix} G_0(r_1,r_1;E) & G_0(r_1,r_2;E) & \cdots & G_0(r_1,r_N;E) \\ G_0(r_2,r_1;E) & G_0(r_2,r_2;E) & \cdots & G_0(r_2,r_N;E) \\ \vdots & \vdots & \ddots & \vdots \\ G_0(r_N,r_1;E) & G_0(r_N,r_2;E) & \cdots & G_0(r_N,r_N;E) \end{pmatrix}. \tag{10}$$

For the position not on the Fe adatoms $r \neq r_i$, the LDOS is given by:

$$\rho(r;E) = -\frac{1}{\pi}\mathrm{Im}(Tr[\mathbf{G}(r,r;E)]). \tag{11}$$

For the LDOS above the corner and edge sites $r = r_i$, we treat them by taking into account the inversion effect [6]. We first calculate the LDOS of the site of concern by assuming the adatom is missing at that site, namely the LDOS of the empty site $\rho(r;E)$. Secondly, we consider the inversion effect caused by the added adatom on this site. Then, the density of state at this adatom can be obtained by the inversion relationship [7, 8]:

$$\rho_a(r;E) = -\frac{1}{\pi}\,\mathrm{Im}\,G_a(E), \tag{12}$$

where Green's function $G_a(E) = \dfrac{1}{E - E_a - \Sigma(E)}$. In it, E_a is the adsorbate energy level of a single adatom and $\Sigma(E) = \Lambda(E) - i\Delta(E)$ is the self-energy where $\Lambda(E) = \dfrac{\Delta_s \ln[(E-E_0)^2 + (\frac{\Gamma}{2})^2]}{2\pi} + const.$ and $\Delta(E) = \Delta_s \rho(r;E)\rho_s(E) + \Delta_b$. Δ_s and Δ_b are the hybridization energy of the adsorbate level with the surface and bulk states, respectively. For the Fe adatom on Ag(111), we adopt the material parameters that were used in Ref. [6], namely, $E_a = 0.21$ eV, $\Delta_s = 0.37$ eV, and $\Delta_b = 0.535$ eV. $\rho_s(E) = \dfrac{1}{2} + \dfrac{\tan^{-1}(\frac{2(E-E_0)}{\Gamma})}{\pi}$ is the surface state of the Ag(111) surface state without any adatom. $\Gamma = 38$ meV is the inverse life time of the surface state [6], and $E_0 = -65$ meV is the surface state onset energy of Ag(111) [9]. Notably, the values for all the parameters mentioned above are imported from References [6, 9]. Thus, there are no tunable parameters in our calculations.

S-3. SPECTRA COMPARISON OF THE CALCULATED AND EXPERIMENTAL RESULTS

For an isolated Fe adatom on the surface, the STM image and *dI/dV* spectrum is shown in Figs. S4(a) and S4(b). The *dI/dV* on top of the Fe adatom shows a resonance around −130 meV. Similar features were observed for Co on Au(111) [10], Cu on Cu(111) [11], and Ag and Co on Ag(111) [8]. These are localized states on top of the transition metal adatoms and are attributed to the strong coupling of the *s* state of the adatoms with the bulk and surface states of the (111) oriented noble metal substrate [12-15]. The calculated LDOS at the Fe adatom is shown in Fig.

S4(c), which shows a close similarity with the experimentally obtained *dI/dV* curve (Fig. S4(b)). The overall bending up of the *dI/dV* curves as compared to the LDOS is due to the bias dependent tunneling matrices [16]. For reference, we also show a typical *dI/dV* curve obtained on a flat Ag(111) terrace, which exhibits a onset energy at −65 meV.

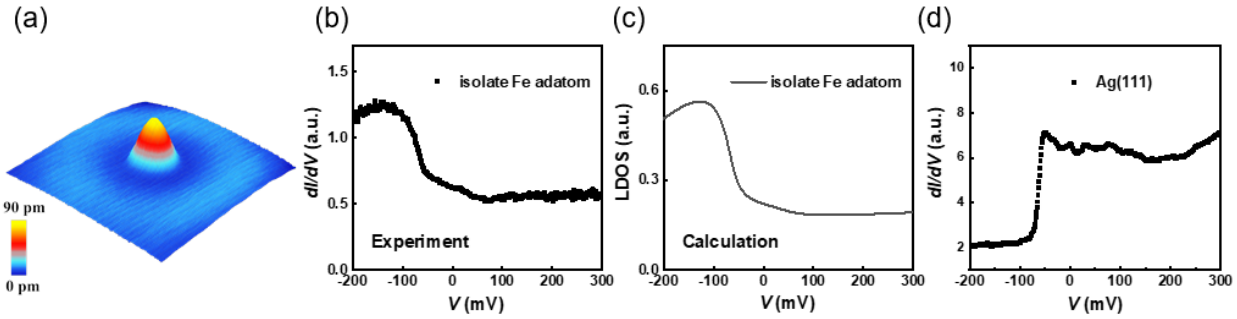

Fig. S4: (a) Morphology of an isolated Fe adatom on a wide Ag(111) terrace. ($V_{bias} = 0.05$ V, $I = 1.0$ nA). (b) The corresponding *dI/dV* spectrum. (c) The calculated LDOS of an Fe single adatom on Ag(111) by means of the Green's function method. (d) A typical experimentally obtained *dI/dV* spectrum of Ag(111) surface.

Figure S5 is the comparison between the experimental *dI/dV* curves and the numerically calculated LDOS via Green's function method. The experimentally raw data of *dI/dV* and *(dI/dV)/(I/V)* obtained with different interatomic distance *r* is shown in Figs. S5(a) and S5(b). They exhibit pronounced peaks with the width increases with decreasing *r*. This can be understood as the surface state contains a lifetime and the scattering caused by the Fe adatoms increases with decreasing *r*. So does the lifetime as well as the peak width. As *r* increases, the peaks interval decreases while the peaks positions gradually move toward lower energy. The calculation results (Fig. S5(c)) show the same trends as the experimental results. To reduce the noise and minimize

the influence of the imperfect positions of Fe adatoms in the lattice sites, we obtained *dI/dV* and *I/V* spectra at different positions of the same type of lattice sites near the middle area of the 4×4 matrix. For each lattice site, the *dI/dV* curves are averaged with more than 20 spectra, and we fitted the average curves with Gaussian function and found the peak positions. The obtained *t* with both $(E_h - E_m)/2$ and $(E_m - E_l)/2$ are shown in Fig. 2(b).

We also quantitatively analyzed the variations of the calculated peaks E_m (green arrow in Fig. S5(c)) and E_h (orange arrow in Fig. S5(c)) with *r*. Table S1 shows the comparison of the fitting parameters in $E = E_0 + C/r^2$ for the peak position E_m and E_h in the calculations and experiments. The calculation results are in good agreement with the experimental results.

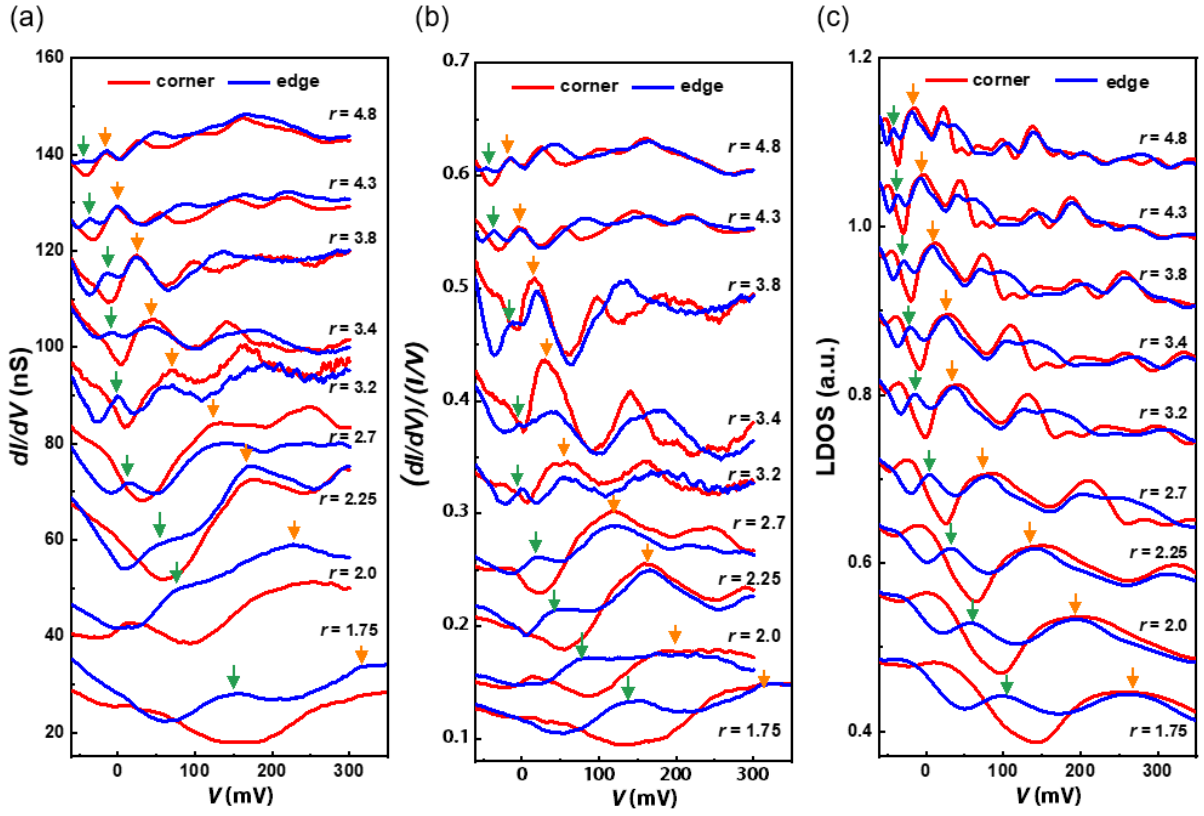

Fig. S5: (a) Raw data of *dI/dV* curves obtained at corner and edge sites with different *r*. (b) *(dI/dV)/(I/V)* spectra. (c) Calculated LDOS at the edge- and corner-sites based on the Green's

function method. The middle- and high-energy peaks positions are marked by green and orange arrows, respectively. Curves in (a), (b) and (c) are shifted for clarity.

Table S1. Fitting parameters in $E = E_0 + C/r^2$ and $\Delta E = E_\Delta + C_\Delta / r^2$ for experiments and calculations.

	E_0 or ΔE (meV)	C or C_Δ (meV•nm^2)
E_l (Exp.)	-58.8 ± 3.3	25.2 ± 19.9
E_m (Exp.)	-62.1 ± 5.2	571.0 ± 34.5
E_m (Calc.)	-64.3 ± 1.2	-505.0 ± 3.4
E_h (Exp.)	-66.5 ± 2.3	1245.5 ± 21.2
E_h (Calc.)	-61.4 ± 1.0	-1010.0 ± 9.2
$(E_h - E_m)/2$ $(E_m - E_l)/2$ (Exp.)	1.0 ± 2.2	273.9 ± 14.5
$(E_h - E_m)/2$ (Calc.)	-1.7 ± 1.2	249.3 ± 8.1

We note that for both the raw data of *dI/dV* spectra and the normalized (*dI/dV*)/(*I/V*) curves, there is a shoulder at the corner site, e.g. around 50 mV for r = 1.75 nm, which also exists in the calculated results with the Green's function method. We find it also exhibits an inverse square relationship with r. To analyze its origin, we plotted the peak energy as the function of r. After a careful analysis, we found that it is related with the eigen energy of the corral marked by the dashed circle in Fig. S6(a). The eigen energy inside of a circular corral is $E_{|n,l\rangle} = E_0 + \hbar^2 k_{n,l}^2 / (2m^*)$, where $k_{n,l} = z_{n,l} / R$ with (n,l) as the quantum number [17]. Here, $\hbar$ is the reduced Planck constant, $z_{n,l}$ is the n^{th} zero crossing of l^{th} order Bessel function and m^* is the effective mass of the surface state. $E_{n,l}$ refers to the state related to the quantum number (n,l). The energy position in the LDOS calculated with the Green's function method agrees well with the eigen energy $E_{1,1}$ of the

marked corral (Fig. S6(b)). Due to the weak strength of the confinement, it appears as a shoulder in LDOS.

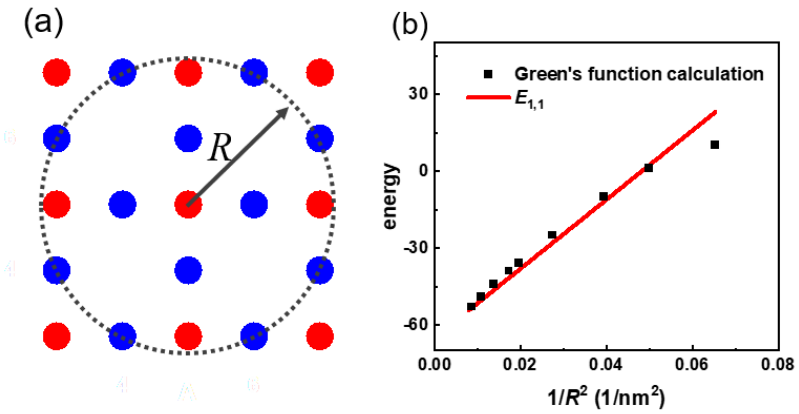

Fig. S6: (a) The outer circular corral with radius R. (b) The comparison of the eigen energy $E_{1,1}$ of the circular corral with the energy of the shoulder at the corner site calculated by Green's function.

Above, we discussed the calculated results for an ideal lattice. In real experiments, it is difficult to position the Fe adatoms to the ideal lattice sites, especially a Lieb lattice has a 4-fold symmetry while the Ag(111) substrate has a 6-fold symmetry. We find that the experimental error margin for positioning the Fe adatoms is ~0.2 nm in lateral. To accommodate the influence of the inaccuracy of Fe adatom positioning, we also made the calculation for a similar structure with the adatom randomly distributed within 0.2 nm away from the ideal lattice site. As shown in Fig. S7, the calculated spectra at both corner and edge sites are similar for the cases with and without disorder. Thus, we conclude that the effect of small disorder is negligibly small.

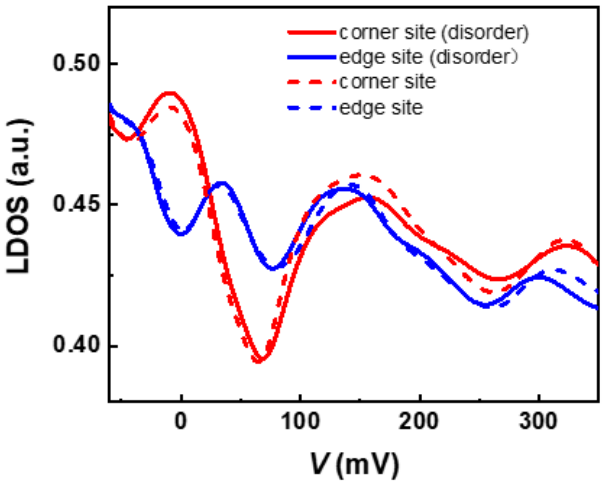

Fig. S7: Comparison of the calculated spectra with and without disorder.

S-4. THE INFLUENCE OF THE UNIT CELL SIZE

According to the Green's function method, we calculated the LDOS for a 4×4 and 5×5 Lieb lattice with $2r$ = 4.5 nm, respectively. We found that the curves are almost the same for these two different sizes (Fig. S8). Thus, we conclude that the 4×4 lattice is sufficient to demonstrate the properties of Lieb lattice. This is in good agreement with previous analysis [18, 19].

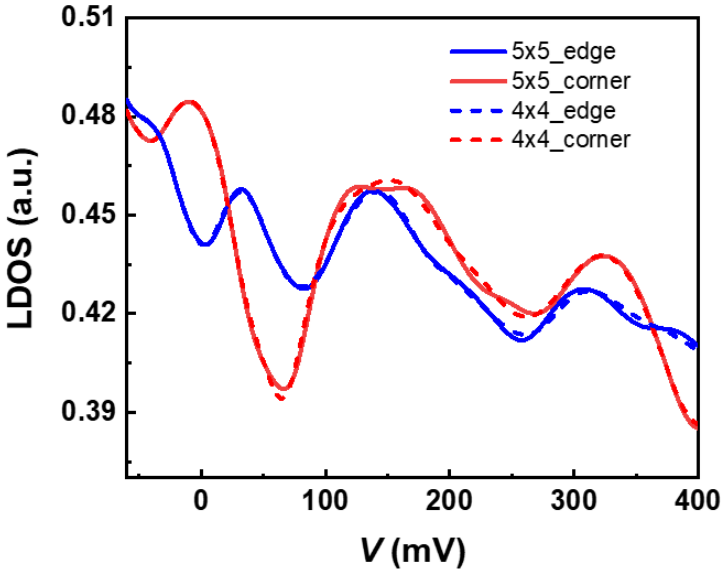

Fig. S8: The calculated LDOS for a 4×4 and 5×5 Lieb lattice via the Green's function method. The lattice constant 2*r* is 4.5 nm.

S-5. LDOS MAPS COMPARISON OF THE CALCULATED AND EXPERIMENTAL RESULTS

To focus our discussion on the distance dependent overlap energy, the LDOS maps in Fig. 3(b) is obtained through the tight-binding calculations only. The scattering of the surface state is neglected. The features at the middle of the Lieb lattice at energy E_m and the ring-shaped features at E_h in Fig. 1(c) are the interference pattern caused by the scattering of the surface state. To further confirm this, we calculated the LDOS map utilizing the Green's function method. As shown in Fig. S9, though not exactly the same, the calculations including the scattering effect do represent close similarity with the experimental observations and the features mentioned above are essentially shown. We note that, in our Green's functions calculation, we only consider the scattering of the surface state by the Fe adatom as well as the hybridization of Fe 4*s* state and the surface state of Ag(111). For more accurate analysis, first-principle calculations may be needed.

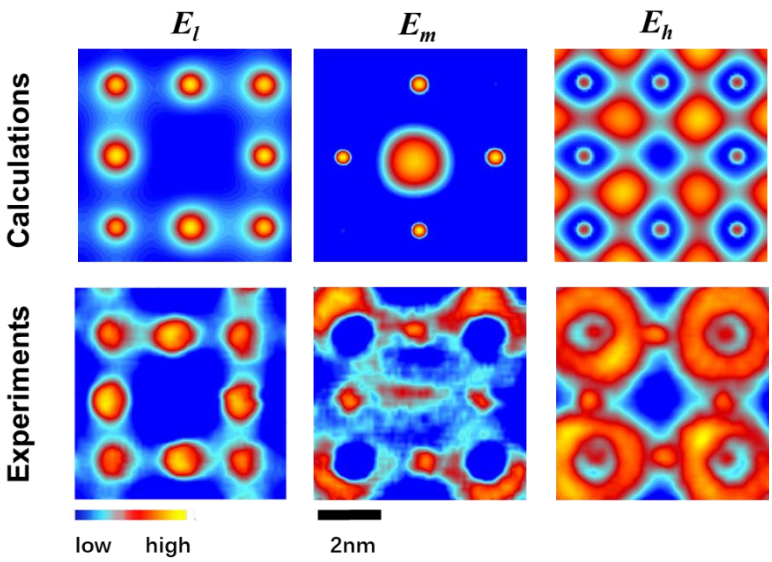

Fig. S9: Comparison of the calculated LDOS maps obtained with Green's function method and the experimental results at E_l, E_m and E_h ($r = 2.25$ nm).

S-6. ARTIFICIAL IRON LIEB LATTICE ON SILVER(100)

We constructed a series of Lieb lattices on Ag(100) in a similar way as we did on Ag(111). The representative topographic image is shown in the inset of (Fig. S10(a)). The *dI/dV* spectra of corner site, edge site and an isolated adatom are almost the same even when we approached a value of *r* of only 1 nm. Namely, no apparent electronic signal of Lieb lattice is observed. Because it is difficult to construct a Lieb lattice with smaller lattice constant, we constructed twin atoms on Ag(100) and investigated the *dI/dV* on top of them with different interatomic separations as shown in (Fig. S10(b)). It is found that there are no apparent differences in *dI/dV* between the spectra obtained on top of the twin atoms with *r* approaching 0.64 nm and that obtained on an isolated adatom (r > 2.8 nm).

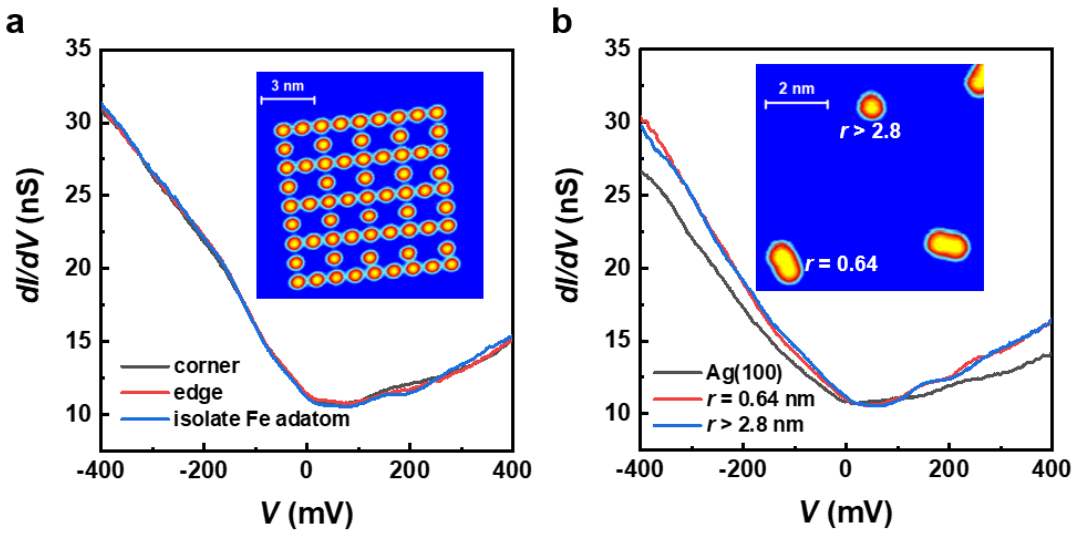

Fig. S10: (a) STM morphologic image and corresponding *dI/dV* spectra at corner- and edge-sites of a 4×4 Lieb lattice constructed by Fe adatoms on Ag(100) with r = 1.25 nm. The spectrum of a single isolated Fe adatom is also included for comparison. (b) STM image and *dI/dV* spectra of Fe adatoms on Ag(100) (STM image: $V_{bias} = 0.5$ V, $I = 1.0$ nA. *dI/dV* spectra: $V_{bias} = 0.1$ V, $I = 1.0$ nA, $V_{mod} = 20$ mV).

Reference

[1] Fiete G A and Heller E J 2003 *Rev. Mod. Phys.* **75** 933-948.
[2] Biswas R R and Balatsky A V 2010 *Phy. Rev. B* **81** 233405.
[3] Fu Z-G, Zhang P, Wang Z and Li S-S 2011 *Phy. Rev. B* **84** 235438.
[4] She J H, Fransson J, Bishop A R and Balatsky A V 2013 *Phy. Rev. Lett.* **110** 026802.
[5] Zheng C, Li Q L, Miao B F, Sun L, Wang R, Li X X and Ding H F 2017 *Phy. Rev. B* **96** 235444.
[6] Li Q L, Li X X, Miao B F, Sun L, Chen G, Han P and Ding H F 2020 *Nat. Commun.* **11** 1400.
[7] Kliewer J, Berndt R and Crampin S 2000 *Phys. Rev. Lett.* **85** 4936-4939.
[8] Limot L, Pehlke E, Kröger J and Berndt R 2005 *Phys. Rev. Lett.* **94** 036805.
[9] Li J T, Schneider W D and Berndt R 1997 *Phys. Rev. B* **56** 7656-7659.
[10] Madhavan V, Chen W, Jamneala T, Crommie M F and Wingreen N S 2001 *Phys. Rev. B* **64** 165412.
[11] Olsson F E, Persson M, Borisov A G, Gauyacq J P, Lagoute J and Fölsch S 2004 *Phys. Rev. Lett.* **93** 206803.
[12] Lazarovits B, Szunyogh L and Weinberger P 2006 *Phys. Rev. B* **73** 045430.
[13] Lounis S, Mavropoulos P, Dederichs P H and Blügel S 2006 *Phys. Rev. B* **73** 195421.

[14] Fernández J, Roura-Bas P and Aligia A A 2021 *Phys. Rev. Lett.* **126** 046801.
[15] Tacca M S, Jacob T and Goldberg E C 2021 *Phys. Rev. B* **103** 245419.
[16] Bonell D 2001 *Scanning Probe Microscopy and Spectroscopy* (Wiley).
[17] Crommie M F, Lutz C P and Eigler D M 1993 *Science* **262** 218-220.
[18] Drost R, Ojanen T, Harju A and Liljeroth P 2017 *Nat. Phys.* **13** 668-672.
[19] Slot M R, Gardenier T S, Jacobse P H, van Miert G C P, Kempkes S N, Zevenhuizen S J M, Smith C M, Vanmaekelbergh D and Swart I 2017 *Nat. Phys.* **13** 672-677.